Draft version November 14, 2012
Preprint typeset using LaTeX style emulateapj v. 12/16/11

REIONIZATION ON LARGE SCALES II: DETECTING PATCHY REIONIZATION THROUGH CROSS CORRELATION OF THE COSMIC MICROWAVE BACKGROUND

A. Natarajan [1], N. Battaglia [1], H. Trac [1], U.-L. Pen [2], A. Loeb [3]

Draft version November 14, 2012

ABSTRACT

We investigate the effect of patchy reionization on the cosmic microwave background temperature. An anisotropic optical depth $\tau(\hat{n})$ alters the TT power spectrum on small scales $l > 2000$. We make use of the correlation between the matter density and the reionization redshift fields to construct full sky maps of $\tau(\hat{n})$. Patchy reionization transfers CMB power from large scales to small scales, resulting in a non-zero cross correlation between large and small angular scales. We show that the patchy τ correlator is sensitive to small root mean square values $\tau_{\rm rms} \sim 0.003$ seen in our maps. We include other secondary anisotropies such as CMB lensing, kinetic and thermal Sunyaev-Zel'dovich terms, as well as the infrared and point source background, and show that patchy reionization may be detected in the low frequency channels ~ 90 GHz, particularly for extended reionization histories. If frequency dependent secondaries can be minimized by a multi-frequency analysis, we show that even small degrees of patchiness can be detected at high significance. In this case, we show that models with different values of $\tau_{\rm rms}$ are distinguishable, even for the same mean value $\langle\tau\rangle$. The patchy τ correlator thus provides information that is complementary to what may be obtained from the polarization and the kinetic Sunyaev-Zel'dovich power spectra.

Subject headings: Cosmology: theory, reionization, cosmic background radiation.

1. INTRODUCTION

Studies of high redshift quasar spectra obtained by the Sloan Digital Sky Survey have found near complete absorption of light blueward of the Lyα line for a quasar at redshift $z = 6.28$ (Fan et al. 2001), i.e. the first detection of the Gunn-Peterson (Gunn & Peterson 1965) trough. Spectroscopy using the Keck telescope (Becker et al. 2001) and the Very Large Telescope (VLT) (Pentericci et al. 2002) confirmed the earlier results. These observations, and the non-detection of the Gunn-Peterson trough for $z < 5.5$ (Becker et al. 2001) imply that the Universe is highly ionized today (Fan et al. 2002).

Evidence for reionization at the 5.5σ level was obtained by the Wilkinson Microwave Anisotropy Probe (WMAP) measurement of the CMB EE polarization power spectrum (Larson et al. 2011a), implying a reionization optical depth $\tau = 0.088 \pm 0.015$. If interpreted in terms of a single step, sudden reionization model, the epoch of reionization $\approx 10.5 \pm 1.2$ (Larson et al. 2011a). The WMAP data is also consistent with an extended reionization scenario (Dunkley et al. 2009).

Reionization began at a redshift $z \sim 20 - 30$ when the first stars were formed. Later, Population II stars, star forming galaxies, and active galactic nuclei completed the process (Tumlinson & Shull 2000; Loeb & Barkana 2001; Barkana & Loeb 2001; Wyithe & Loeb 2003; Ciardi et al. 2003; Sokasian et al. 2003). Due to the very large photoionization cross section at energies $\gtrsim 13.6$ eV, ultraviolet (UV) photons are absorbed by gas in the immediate vicinity of the sources, forming "bubbles" of ionized Hydrogen. This leads to large spatial fluctuations in the ionized fraction, and reionization is said to be *patchy*. The bubbles grow and eventually merge, resulting in a uniformly reionized Universe at $z \sim 6$.

If reionization is patchy, scattering of CMB photons varies with the line of sight, introducing secondary anisotropies. Zahn et al. (2005) and McQuinn et al. (2006) used analytical models and numerical simulations to study patchy reionization. Weller (1999) and Liu et al. (2001) computed the modification to the EE polarization caused by inhomogeneous reionization, and found the effect to be small, though potentially detectable by future observations. Hu (2000) showed that inhomogeneities in the free electron density could generate B mode polarization through Thomson scattering, while Doré et al. (2007) found that the polarization power due to patchy τ has a unique signature. It was shown by Dvorkin et al. (2009) that in addition to B modes being created by inhomogeneous Thomson scattering, patchy screening of the primary E mode leads to B mode polarization. Dvorkin & Smith (2009) described an optimal quadratic estimator that could reconstruct patchy reionization from the CMB. Mortonson & Hu (2010) used the South Pole Telescope (SPT) limits on secondary anisotropies at $l = 3000$ to infer that fluctuations in the optical depth are utmost a few percent of the mean value $\langle\tau\rangle$. Recent observations by the SPT collaboration (Zahn et al. 2012) have placed an upper limit on the patchy kinetic Sunyaev-Zel'dovich (kSZ) power at $l = 3000$ to be $D_{3000}^{\rm patchy} < 4.9\,\mu{\rm K}^2$ at the 95% confidence level when the degree of angular correlation between the thermal Sunyaev-Zel'dovich (tSZ) and the cosmic infrared background (CIB) is allowed to vary. The

[1] McWilliams Center for Cosmology, Carnegie Mellon University, Department of Physics, 5000 Forbes Ave., Pittsburgh PA 15213, USA
[2] Canadian Institute for Theoretical Astrophysics, University of Toronto, 60 St. George Street, Toronto, ON M5S 3H8, Canada
[3] Institute for Theory & Computation, Harvard University, 60 Garden Street, Cambridge, MA 02138, USA

SPT results (Zahn et al. 2012) imply that reionization ended at $z > 5.8$ at 95% confidence (accounting for the tSZ-CIB correlation), in good agreement with quasar observations.

In Battaglia et al. (2012b) (henceforth Paper I), we described a new method for modeling inhomogeneous reionization on large scales. In the present article, we study the effect of inhomogeneous reionization (henceforth patchy τ) on the CMB temperature power spectrum. We present a technique that can detect patchy τ for root mean square $\tau_{\rm rms}$ as small as $\lesssim 0.003$, as seen in our maps. We then include various secondary anisotropies and show that patchy τ may still be detected for observations made at low frequencies. If frequency dependent secondaries can be minimized by a multi-frequency analysis, much more stringent constraints on reionization may be obtained. Finally, we present our conclusions. We adopt the following cosmological parameters consistent with the WMAP observations (Larson et al. 2011b): $\Omega_\Lambda = 0.73, \Omega_{\rm b} = 0.045, h = 0.7, n_{\rm s} = 0.96$, and $\sigma_8 = 0.80$.

2. SECONDARY ANISOTROPIES DUE TO PATCHY τ

The CMB temperature as seen by an observer on earth in the direction $\hat{n}$ may be written as the sum of 2 terms:

$$T(\hat{n}) = \mathcal{T}_1(\hat{n}) + \mathcal{T}_2(\hat{n}). \quad (1)$$

$T(\hat{n})$ represents the CMB brightness temperature in the Rayleigh-Jeans limit. $\mathcal{T}_1(\hat{n})$ describes CMB photons that do not interact with free electrons, and therefore represent the temperature on the decoupling surface in the direction $\hat{n}$. Let $\tau(0, \hat{n})$ be the optical depth due to scattering in the direction $\hat{n}$:

$$\tau(l, \hat{n}) = \sigma_{\rm T} \int_l^{l_*} dl'\, n_{\rm e}(l', \hat{n}), \quad (2)$$

where $dl = c\,dt$ is the proper distance along the line of sight. $l = 0$ represents the observer, and l_* is the decoupling surface. $n_{\rm e}(l, \hat{n})$ is the free electron number density at l in the direction $\hat{n}$, and $\sigma_{\rm T}$ is the Thomson scattering cross section. Let $\theta(\hat{n})$ be the fractional change in the CMB temperature, and let T_0 be the CMB temperature averaged over all angles. $\mathcal{T}_1(\hat{n})$ is then given by:

$$\mathcal{T}_1(\hat{n}) = T_0\,[1 + \theta(\hat{n})]\, e^{-\tau(\hat{n})}. \quad (3)$$

The term $\mathcal{T}_2(\hat{n})$ describes CMB photons that scatter with free electrons. These photons originate at different points on the decoupling surface, and scatter into the line of sight $\hat{n}$. $\mathcal{T}_2(\hat{n})$ thus samples the entire decoupling surface, but depends on the line of sight due to the anisotropy in the ionized fraction.

$$\mathcal{T}_2(\hat{n}) = 2T_0 \int_0^{l_*} dl\; n_{\rm e}(l, \hat{n})\; \left\langle \frac{d\sigma}{d\mu}\; [1 + \theta(\hat{n}')]\, e^{-\tau(\hat{n}', l)} \right\rangle. \quad (4)$$

The angle brackets indicate an average over different lines of sight. $\mu = \hat{n} \cdot \hat{n}'$, and the factor of 2 arises from the relation $\int_{-1}^{1} d\mu\, f(\mu) = 2\langle f(\mu)\rangle$. The differential cross section at low energies is:

$$d\sigma/d\mu = (3/8)\sigma_{\rm T}(1 + \mu^2). \quad (5)$$

Let us express the optical depth $\tau(\hat{n})$ as the sum of an isotropic term $\tau_0(l)$ and an angle dependent term $\eta(l, \hat{n})$, i.e. $\tau(l, \hat{n}) = \tau_0(l) + \eta(l, \hat{n})$. $\mathcal{T}_2(\hat{n})$ is then given by

$$\begin{aligned}\mathcal{T}_2 &\approx \frac{3}{4} T_0\, \sigma_{\rm T} \int dl\; n_{\rm e}(l) e^{-\tau_0(l)} \left\langle \left[1 + \mu^2\right] e^{-\eta\left(\hat{n}', l, l_*\right)} \right\rangle \\ &= T_0\, \sigma_{\rm T} \int dl\, n_{\rm e}(l) e^{-\tau_0(l)}\; [1 + f_1 + f_2]\,. \end{aligned} \quad (6)$$

In Equation (6), we have assumed that $\theta(\hat{n})$ and $\eta(\hat{n})$ are uncorrelated, and hence $\langle\theta\eta\rangle = 0$. We have also ignored $\mu^2\theta$ compared to μ^2. The terms $f_1, f_2 \ll 1$ are given by

$$\begin{aligned} f_1 &= \frac{3}{4}\left[\langle e^{-\eta}\rangle - 1\right] \approx \frac{3}{8}\langle\eta^2\rangle + \cdots \\ f_2 &= \frac{3}{4}\left[\langle\mu^2 e^{-\eta}\rangle - \frac{1}{3}\right] \approx -\frac{3}{4}\langle\mu^2\eta\rangle + \cdots \end{aligned} \quad (7)$$

Typically, we find $\langle\eta^2\rangle^{1/2}, \langle\mu^2\eta\rangle \ll \tau_0$. From Equation (6) and Equation (2), we find to lowest order:

$$\mathcal{T}_2 = T_0\left[1 - e^{-\tau(\hat{n})}\right]. \quad (8)$$

The CMB temperature in the direction $\hat{n}$ is

$$T(\hat{n}) = \mathcal{T}_1 + \mathcal{T}_2 = T_0\left[1 + \theta(\hat{n})\, e^{-\tau(\hat{n})}\right]. \quad (9)$$

The fractional CMB temperature after scattering $\theta_{\rm obs}(\hat{n})$ to lowest order is given by

$$\theta_{\rm obs}(\hat{n}) = \theta(\hat{n})\, e^{-\tau(\hat{n})}. \quad (10)$$

The total CMB TT power spectrum may be obtained by performing a multipole decomposition of $\theta_{\rm obs}(\hat{n})$.

3. METHODOLOGY

We have developed a unique technique (described in Paper I) where the non-linear density field can be filtered with a simple parametric relation to directly obtain the reionization-redshift field. A particle-particle-particle-mesh ($\rm P^3M$) N-body code is used to evolve 2048^3 dark matter particles in a 2000 Mpc/h box and generate nonlinear density fields $\rho(\vec{x})$ and velocity fields $\vec{v}(\vec{x})$ down to $z = 5.5$. Our semi-analytic model for reionization is based on results from radiative transfer hydrodynamic simulations (Trac et al. 2008; Battaglia et al. 2012b). We track when a gas cell first becomes more than 90% ionized and construct a 3D reionization-redshift field $z_{\rm r}(\vec{x})$ in parallel with the density field $\rho(\vec{x})$. Let us define the fluctuations in the matter density and the reionization-redshift fields as follows:

$$\begin{aligned} \delta_{\rm m}(\vec{x}) &= \frac{\rho(\vec{x}) - \bar{\rho}}{\bar{\rho}} \\ \delta_{\rm z}(\vec{x}) &= \frac{[1 + z_{\rm r}(\vec{x})] - [1 + \bar{z}_{\rm r}]}{1 + \bar{z}_{\rm r}}. \end{aligned} \quad (11)$$

From the Fourier transform of these quantities, we construct the bias and the cross-correlation functions:

$$\begin{aligned} b_{\rm zm}(k) &= \sqrt{\frac{\langle\delta_{\rm z}\delta_{\rm z}\rangle}{\langle\delta_{\rm m}\delta_{\rm m}\rangle}} \\ r_{\rm zm}(k) &= \frac{\langle\delta_{\rm z}\delta_{\rm m}\rangle}{\sqrt{\langle\delta_{\rm z}\delta_{\rm z}\rangle\langle\delta_{\rm m}\delta_{\rm m}\rangle}} \end{aligned} \quad (12)$$

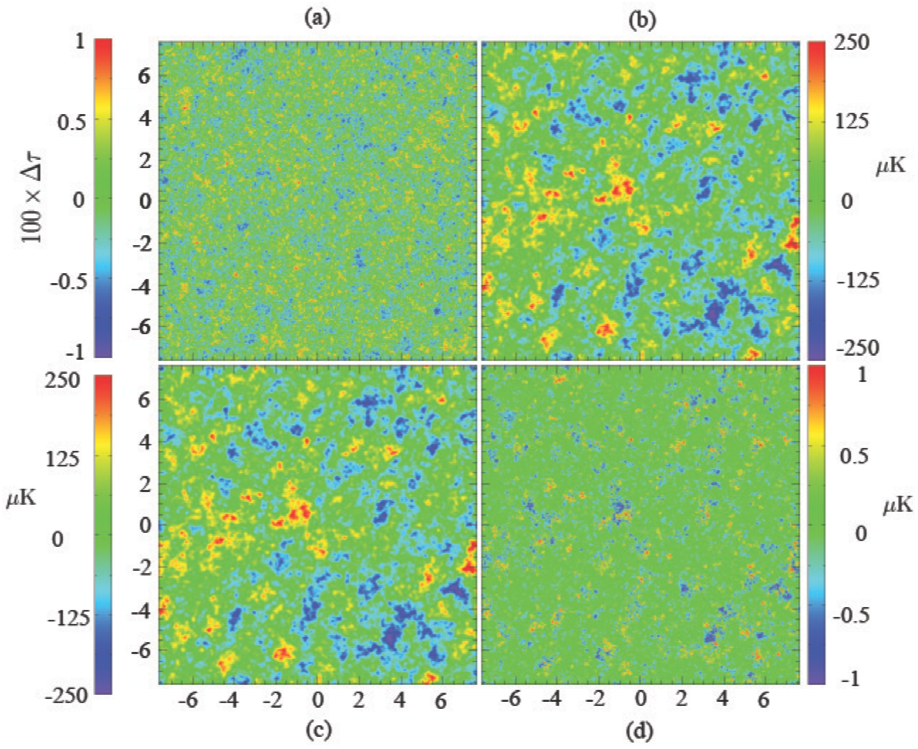

FIG. 1.— Panel (a) shows fluctuations in the optical depth, in a 15° × 15° region of the sky, from our maps. Panel (b) is a HEALPix realization of the primary CMB fluctuations. Panel (c) shows the CMB fluctuations with the effect of patchy τ included, while panel (d) shows only secondary CMB fluctuations due to the patchy τ effect. Fluctuations in the τ map are on much smaller scales than the CMB fluctuations. As seen from panels (b) and (c), the contribution due to patchy τ is small.

We find that the density and reionization fields are highly correlated on comoving scales > 1 Mpc/h (see Paper I). $\delta_z(k)$ may thus be obtained by applying a calibrated bias to $\delta_m(k)$.

Full sky HEALPix (Nside = 4096) maps of the patchy Thomson optical depth and kinetic Sunyaev-Zel'dovich effect are then constructed by raytracing through the simulated lightcone. Panel (a) of Figure 1 shows a 15° × 15° section of the τ map. The mean value of optical depth for this map is $\langle\tau\rangle = 0.083$, while the root mean square value $\tau_{\rm rms} = 0.0027$. Panel (b) shows a realization of the CMB sky, computed using the HEALPix package[4](Górski et al. 2005). As can be seen, the τ fluctuations are on much smaller scales than the CMB fluctuations. Panel (c) shows the CMB fluctuations with patchy τ included, while panel (d) shows the contribution due to patchy τ. From (b) and (c), we see that the patchy τ contribution is small.

We use a simple parametric form for the bias function:

$$b_{\rm zm} = \frac{b_{\rm o}}{(1 + k/k_{\rm o})^{\alpha}}. \qquad (13)$$

The bias approaches a constant on the largest scales $b_{\rm zm} \to 1/\delta_{\rm c} = 1/1.686$ (Barkana & Loeb 2004). The bias parameter $b_{\rm zm}$ contains 3 variables $b_{\rm o}$, $k_{\rm o}$, and α. $b_{\rm o}$ is determined from analytical arguments in Barkana & Loeb (2004), while $k_{\rm o}$, and α are found from simulations. Together with the redshift of 50% reionization ($\bar{z}$), the parameters $k_{\rm o}$ and α determine the degree of patchiness.

[4] HEALPix may be downloaded from http://healpix.jpl.nasa.gov

Figure 2 shows $\tau_{\rm rms} \times 10^3$ for different values of $k_{\rm o}$ and α, for a fixed value of $\bar{z} = 10$. Thus, $\tau_{\rm rms} < 4\%$ of $\langle\tau\rangle$, for $\bar{z} = 10$.

We consider two different reionization scenarios, shown in panel (a) of Figure 3. The solid (black) curve shows our fiducial reionization model in which the Universe is 50% reionized at $\bar{z} = 10$, with $\tau_{\rm rms} = 0.0027$. The dot-dashed (orange) curve is also plotted for $\bar{z} = 10$, but for a more extended reionization history, and a correspondingly larger $\tau_{\rm rms} = 0.0031$ (We choose $\bar{z} = 10$ for consis-

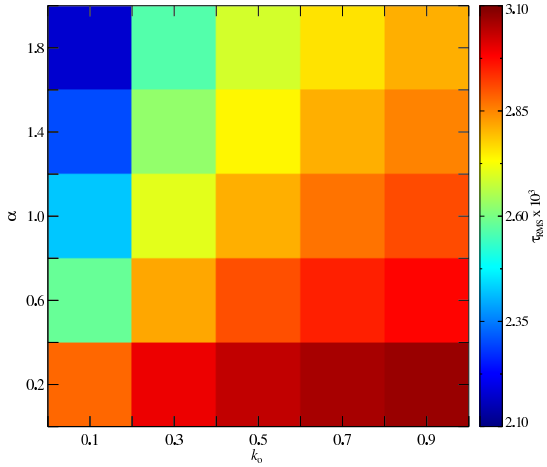

FIG. 2.— $\tau_{\rm rms} \times 10^3$, shown for different values of α and k_0. The redshift of 50% reionization $\bar{z} = 10$. $\tau_{\rm rms} < 4\%$ of the mean optical depth $\langle\tau\rangle$ for $\bar{z} = 10$.

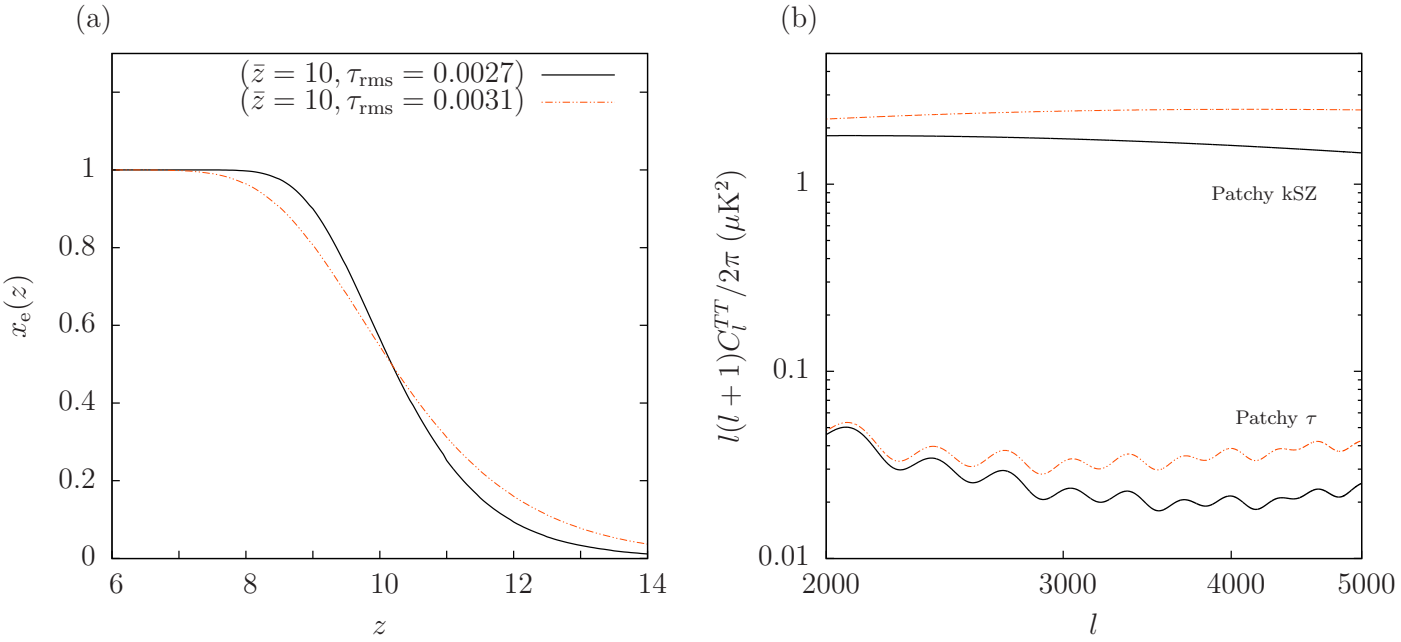

FIG. 3.— Two different reionization models are shown (panel a) with the corresponding patchy τ and patchy kSZ ($z > 5.5$) contributions (panel b). The homogeneous kSZ ($z < 5.5$) is not shown.

tency with the WMAP measured value of optical depth). Decreasing $\bar{z}$ while keeping the duration of reionization fixed would decrease both $\langle\tau\rangle$ and $\tau_{\rm rms}$. The panel on the right shows the secondary CMB power due to patchy τ compared with the secondary power due to patchy kSZ. The homogeneous kSZ power for $z < 5.5$ is the same for all reionization models, and is not shown here. We note that the patchy τ contribution is extremely small.

Figure 4 shows the different components of the CMB temperature power spectrum, along with Atacama Cosmology Telescope (ACT) data (Dunkley et al. 2011; Das et al. 2011) at 148 GHz and South Pole Telescope (SPT) data (Reichardt et al. 2012) at 150 GHz. The solid black curve represents the primary CMB, while the solid red curve is the contribution due to patchy τ, for a model characterized by a reionization redshift $\bar{z} = 10$, mean $\langle\tau\rangle = 0.083$, and patchiness $\tau_{\rm rms} = 0.0027$. Also shown are the contributions from patchy + homogeneous kSZ, the expected tSZ power (at 148 GHz), the contribution from CMB lensing, and the power from IR + point sources (at 148 GHz). At multipole $l = 3000$, the patchy kSZ ($z > 5.5$) contributes $\approx 1.75\,\mu{\rm K}^2$ (Battaglia et al. 2012a), the homogeneous kSZ ($z < 5.5$) power is $\approx 1.48\,\mu{\rm K}^2$ (Trac et al. 2011), and the tSZ $\approx 6.24\,\mu{\rm K}^2$ (Trac et al. 2011). In contrast, the patchy τ contribution is only $\approx 0.023\,\mu{\rm K}^2$.

In an attempt to constrain $\tau_{\rm rms}$, we perform a maximum likelihood analysis using CMB data from the ACT (Dunkley et al. 2011; Das et al. 2011) and WMAP (Larson et al. 2011b) experiments, and the publicly available CMB Boltzmann code CLASS (Lesgourgues 2011; Blas et al. 2011). We find that current CMB power spectrum data is insensitive to realistic values of patchiness. The future ACTPol experiment is expected to cover 4000 square degrees of the sky with a noise equivalent power ~ 20 aW/$\sqrt{\rm Hz}$, and a beam width ≈ 1.4 arcmin (148 GHz channel) (Niemack et al. 2010). The future SPTPol experiment is expected to cover ~ 625 square degrees of the sky, with a noise equivalent power ~ 53.5 aW/$\sqrt{\rm Hz}$, and a beam width of ~ 1 arcmin (150 GHz channel) (Bleem et al. 2012). With these specifications, we expect the ACTPol and SPTPol experiments to be more sensitive to patchy τ and patchy kSZ. We do not expect a significant improvement from the Planck mission, owing to the large (~ 5 - 7') beam width (Lamarre et al. 2010), which limits CMB measurements

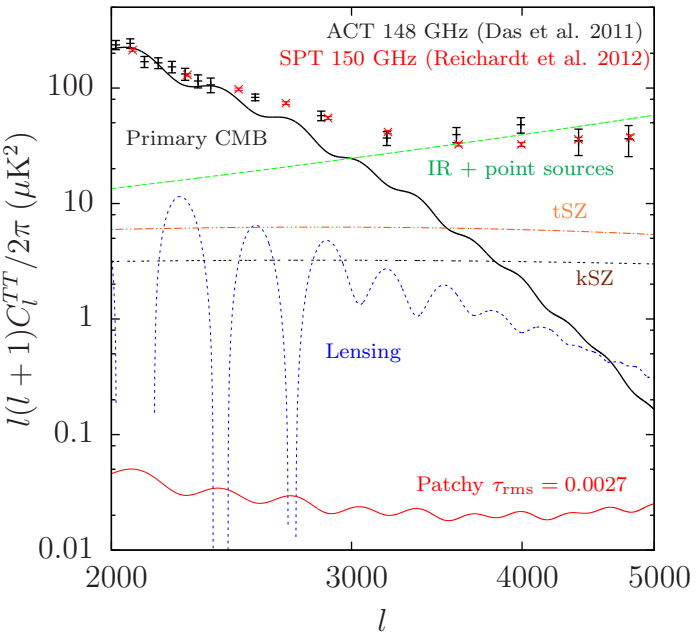

FIG. 4.— The primary CMB (solid, black), ACT (148 GHz) (Dunkley et al. 2011; Das et al. 2011) and SPT (150 GHz) (Reichardt et al. 2012) data points, and various secondary components, at 148 GHz. The contribution from patchy τ is shown in red, for a reionization model with $\bar{z} = 10, \tau_{\rm rms} = 0.0027$.

to scales $l < 2000$. In the next section, we will discuss a much improved technique for detecting patchy reionization.

4. DETERMINING PATCHY τ FROM THE TEMPERATURE MAPS

We now discuss a different approach to detecting the presence of patchy reionization. We construct a simple estimator that is far more sensitive to non-zero $\tau_{\rm rms}$ than the power spectrum. Since the damping term $\exp -\tau(\hat{n})$ multiplies the primary CMB temperature T [Equation (10)], the effect of patchy reionization is largest when $|T|$ is large. From Figures 1 and 4, we see that patchy reionization alters the primary CMB only on very small scales. We therefore filter the CMB map (which includes the effect of patchy τ) into 2 maps: (i) A map f with information only on large scales, i.e. multipoles $l < l_{\rm boundary1}$, and (ii) A map g with information only on small scales, $l > l_{\rm boundary2}$. Due to computational limitations, and to limit contamination of the small scale map by the large IR background, we set $l_{\rm max} = 5000$ as the maximum multipole moment of interest. The 2 maps are then squared:

$$\begin{aligned} f &= T^2(l < l_{\rm boundary1}) \\ g &= T^2(l > l_{\rm boundary2}). \end{aligned} \quad (14)$$

We compute the cross correlation $\langle \delta f\, \delta g \rangle$, which we call the patchy τ correlator. $\delta f = f - \langle f \rangle$ and $\delta g = g - \langle g \rangle$ are fluctuations in the squared CMB temperature obtained from the filtered maps. The angle brackets denote an average over the map. We use the LensPix[5] (Lewis 2005) (see also Das & Bode (2008) for a detailed description of CMB lensing) and HEALPix packages to generate 5 different realizations of the lensed and unlensed CMB. We account for patchy reionization by multiplying the unlensed CMB by the damping term $\exp -\tau(\hat{n})$ for a given reionization scenario. Secondary anisotropies such as CMB lensing, kSZ, tSZ and the infrared and point source background are then added to the map. The combined map is filtered using HEALPix programs, to obtain a map with information only on large scales $l < l_{\rm boundary1}$, and a second map containing information only on small scales $l > l_{\rm boundary2}$.

Frequency dependent secondary effects may be reduced by observing the CMB at multiple frequencies. The Planck Satellite, expected to release data in early 2013 consists of a Low Frequency Instrument (LFI) (Mandolesi et al. 2010) which observes the CMB at frequencies 30 GHz, 44 GHz, and 70 GHz, as well as a High Frequency Instrument (HFI) (Lamarre et al. 2010) sensitive to frequencies 100 GHz, 143 GHz, 217 GHz, 353 GHz, 545 GHz, and 857 GHz. The beam width varies from 33 arc minutes at 30 GHz to 5 arc minutes at 857 GHz (Mandolesi et al. 2010; Lamarre et al. 2010). On relatively large scales, one could use observations at these 9 frequencies to remove frequency dependent secondary contributions. On small scales ($l > 3000$), one must use observations from other experiments with better angular resolution such as ACT, SPT, and the upcoming ACTPol, and SPTPol experiments. The ACT experiment is sensitive to frequencies 148 GHz and 219 GHz (Hlozek et al. 2012), while the SPT experiment measures the CMB at frequencies 95 GHz, 150 GHz, and 220 GHz (Reichardt et al. 2012). Let us expand δf and δg into frequency independent and frequency dependent terms as:

$$\begin{aligned} \delta f &= \delta f_0 = [f - \langle f \rangle]_0 \\ \delta g &= (\delta g_0 + \delta g_\nu) = [g - \langle g \rangle]_0 + [g - \langle g \rangle]_\nu, \end{aligned} \quad (15)$$

where the subscript 0 denotes a frequency independent contribution (the primary CMB, patchy τ, lensing, and kSZ), while the subscript ν denotes a frequency dependent contribution (such as the tSZ effect, and the infrared and point source background). In Equation (15), we have made the assumption that frequency dependent terms can be removed from the large scale map using the many frequency channels of the Planck experiment. A similar assumption cannot be made for the small scale map however, as current and upcoming arcminute scale experiments measure the CMB at only 3 frequencies. We thus include the tSZ effect as well as the IR and point source background in the small scale map. The patchy τ correlator $\langle \delta f\, \delta g \rangle$ may then be decomposed into frequency independent and frequency dependent terms:

$$\begin{aligned} \langle \delta f\, \delta g \rangle &= \langle \delta f_0\, \delta g_0 \rangle + \langle \delta f_0\, \delta g_\nu \rangle \\ &= A + B(\nu). \end{aligned} \quad (16)$$

The frequency independent term $A \neq 0$ since the patchy τ and CMB lensing contributions lead to a non-zero cross correlation between the squared large scale and small scale maps. The frequency dependent term $B(\nu)$ is zero since none of the frequency dependent secondaries are expected to be correlated with the primary CMB. In practice $B(\nu)$ will not be zero due to noise. By computing the cross correlation at different frequencies, it may be possible to overcome noise, thus minimizing frequency dependent contaminations.

Figure 5 shows the patchy τ correlator (in units of μK^4) with and without the effect of patchy τ. $\langle \delta f\, \delta g \rangle$ is averaged over 5 CMB realizations, and plotted as a function of $l_{\rm boundary1}$ (largest multipole value for the large scale map). We set $l_{\rm boundary2} = 3000$ (smallest multipole value for the small scale map) since the patchy τ contribution is much smaller than the primary CMB at smaller multipoles, and the contribution from the IR background is prohibitively large at much larger multipoles. We choose $l_{\rm boundary1} \neq l_{\rm boundary2}$ in order to minimize contamination of the large scale map by secondary components. The error bars denote the root mean square (RMS) value of the different CMB realizations.

The top row of Figure 5 (panels (a) and (b)) shows the ideal scenario in which there exist only frequency independent contributions namely CMB lensing and kSZ. Panel (a) (top left) considers our fiducial reionization model characterized by ($\bar{z} = 10, \tau_{\rm rms} = 0.0027$), while panel (b) (top right) corresponds to the extended reionization history ($\bar{z} = 10, \tau_{\rm rms} = 0.0031$). Since different multipoles of the primary CMB provide independent information, the correlation between large and small scale maps is zero for the primary CMB. Including the effect of CMB lensing however results in a non-zero cross correlation. This is expected as lensing of the CMB results in a redistribution of power, transferring CMB power from large scales to small scales. The cross correlation due to lensing is negative for small $l_{\rm boundary1}$, and in-

[5] LensPix available at http://cosmologist.info/lenspix

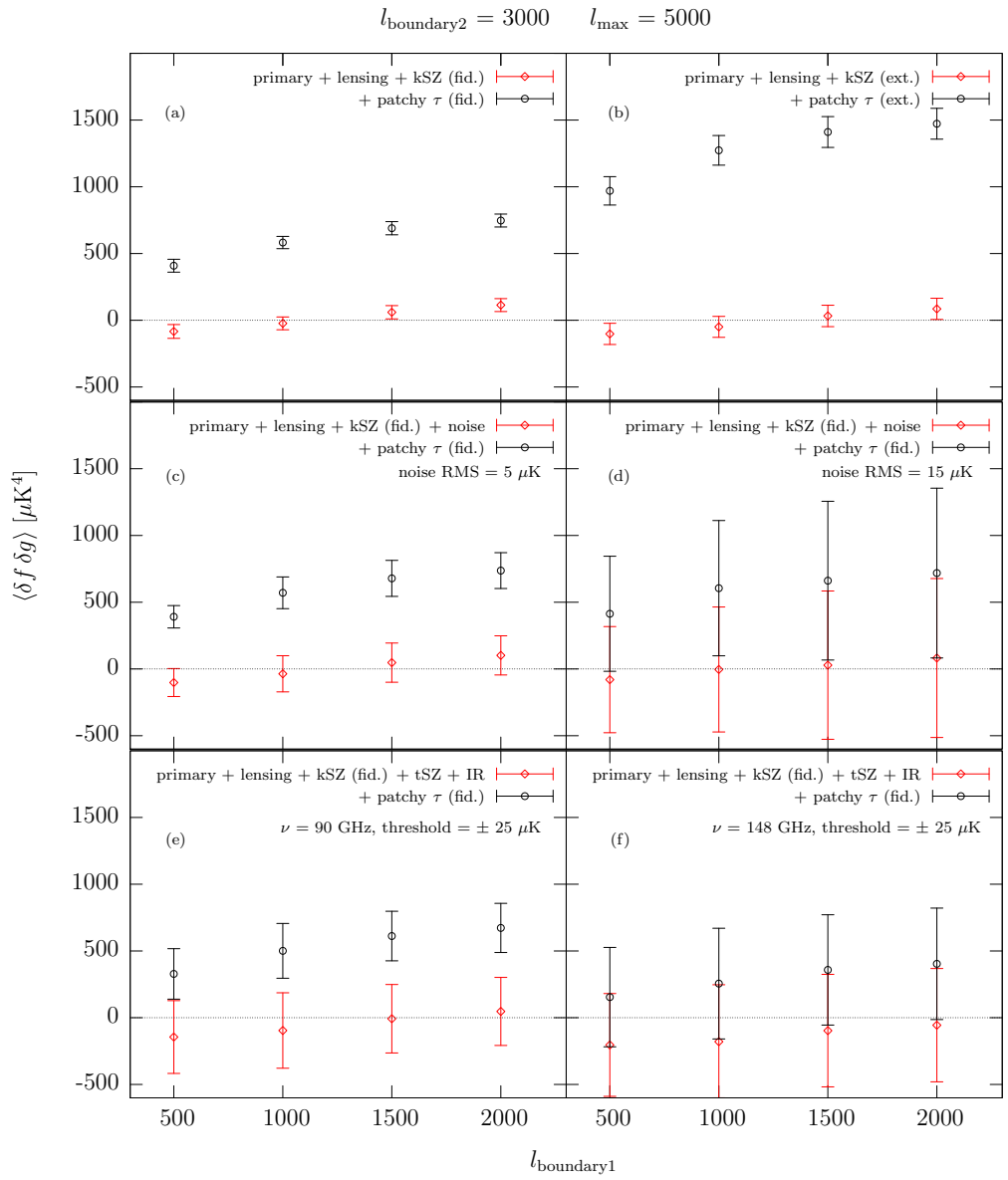

FIG. 5.— The patchy τ correlator as a function of $l_{\rm boundary1}$. The top 2 panels include only frequency independent components, namely CMB lensing and kSZ. Patchy τ can be detected at high confidence, and the magnitude of the correlator can be used to constrain extended reionization histories. The center 2 panels show the correlator with gaussian noise included, to account for residuals after frequency dependent secondaries have been subtracted. The bottom 2 panels include the tSZ and the IR at frequencies 90 GHz and 148 GHz. A statistically significant detection of patchy τ can be made in the 90 GHz channel. Zero correlation is shown for reference (thin broken line).

creases, passing through zero at $l_{\rm boundary1} \sim 1200$. The patchy τ term is similarly correlated. The cross correlation due to patchy τ is always positive and increases with $l_{\rm boundary1}$. Moreover the patchy τ terms contributes significantly more to the cross correlation than the lensing term. Thus, with only the lensing and kSZ contributions, one can detect patchy reionization at high significance by computing the cross correlation between the squared large and small scale maps. From the magnitude of the patchy τ correlator (panels (a) and (b)), we obtain information regarding the reionization history. It may thus be possible to distinguish different reionization models *that predict the same mean optical depth* by computing the patchy τ correlator, provided the models predict different values of $\tau_{\rm rms}$. This method is complementary to measuring the CMB polarization power spectrum which is sensitive to variations in $\langle \tau \rangle$, but cannot distinguish reionization models with different $\tau_{\rm rms}$. We see no statistically significant cross correlation with the kSZ which merely serves to increase the size of the fluctuations about the mean.

Panels (c) and (d) in the middle row show the effect of adding gaussian distributed random noise with zero mean to the small scale CMB maps. The purpose of adding noise is to mimic the effect of frequency dependent secondaries that are still present after a multi-frequency analysis has been employed to minimize the contribution from these components. No noise is added to the large scale maps since upcoming experiments such as the Planck mission are expected to measure the CMB

temperature to high accuracy on scales $l \lesssim 2000$ (cosmic variance is accounted for, by considering many realizations of the CMB sky). Panel (c) shows the cross correlation in the presence of added noise with an RMS temperature of 5 μK/pixel, while panel (d) considers a larger RMS noise temperature of 15 μK/pixel. We will see that these noise values are representative of the residuals from the tSZ and IR contaminations, after bright pixels are masked out. A more thorough multi-frequency analysis of the tSZ and IR contributions will likely yield smaller residuals. Each pixel in our maps has an area of 0.74 arcmin^2. The addition of gaussian noise does not affect the mean value of $\langle \delta f\, \delta g \rangle$, but it significantly increases the variance. It is still possible to distinguish patchy τ in panel (c) with 5 μK of added noise. On the other hand, with 15 μK of added noise, panel (d) shows no significant correlation. We thus need to ensure that secondary components and other sources of noise contribute $\lesssim 5-10\,\mu$K for a detection of patchy τ with high significance.

The bottom two panels ((e) and (f)) study the effect of frequency dependent secondary effects in the small scale maps. We have included the contribution from the tSZ (Trac et al. 2011) and the IR + point source background (Sehgal et al. 2010)[6] at frequencies 90 GHz (panel (e)) and 148 GHz (panel (f)). For simplicity, we do not include contributions from radio galaxies or galactic dust. We apply a mask to the small scale map by setting to zero, any pixel whose temperature is greater than $25\,\mu$K or smaller than $-25\,\mu$K. This threshold value was chosen to be representative of the sensitivity of ongoing and upcoming CMB experiments. The ACT mission has achieved a noise level between 25 and 40 μK$-$arcmin (Hlozek et al. 2012), while the noise level achieved by the SPT mission $\sim 18\,\mu$K$-$arcminute (the future ACTPol mission (Niemack et al. 2010) expects to achieve a sensitivity of $20\,\mu$K$-$arcmin for the wide survey, and $3\,\mu$K$-$arcmin for the deep survey). (The pixel area in our maps is 0.74 arcmin^2. The noise in the relevant band, i.e. $l_{\rm boundary2} < l < l_{\rm max}$ may be smaller than the figure quoted by ACT and SPT, for scale independent noise). The frequency independent contributions due to CMB lensing and the kSZ are included in both large scale and small scale maps. We do not mask any pixel in the large scale map.

At a frequency of 90 GHz, the tSZ contributes an RMS temperature $\sim 6.8\,\mu$K, while the IR and point source background contributes $\sim 5.7\,\mu$K (RMS temperatures are computed at all scales, the RMS in the restricted band is smaller). With these two sources of background included, we are still able to distinguish the effect of patchy τ, albeit with lower confidence (panel (e)) compared to panel (a). With increase in frequency, the tSZ contribution decreases, but this is compensated by a large increase in the IR background. At 148 GHz, the tSZ contributes an RMS temperature $\sim 4.2\,\mu$K, while the IR and point source background contributes $\sim 15\,\mu$K. The background is now dominated by IR, and we are unable to make a statistically significant detection of patchy τ (panel (f)). The magnitude of the patchy τ correlator is significantly decreased since there are many pixels that exceed the threshold of $\pm$ 25 μK. The IR contribution dramatically increases at still higher frequencies. At 219 GHz, the IR contributes $\sim 49\,\mu$K, completely overwhelming the small signal due to patchy τ. Nevertheless, the tSZ contribution is nearly zero at this frequency, and observations at this frequency may be used to detect and minimize the tSZ contribution at lower frequencies. Future experiments that observe the CMB at multiple frequencies will help in characterizing the behavior of large secondary anisotropies. The PIXIE (Primordial Inflation Explorer) satellite (Kogut et al. 2011) is a full sky experiment planned for 2017 that can observe the CMB on large scales. The instrument has 400 frequency channels from 30 GHz to 6 THz, with a low noise equivalent power ~ 70 aW$/\sqrt{\rm Hz}$, and will greatly improve our understanding of frequency dependent contaminations on large scales.

[6] IR maps may be downloaded from http://lambda.gsfc.nasa.gov/toolbox/tb_cmbsim_ov.cfm

5. CONCLUSIONS

We investigated the effect of patchy reionization on the CMB temperature. We showed that the anisotropy in the optical depth $\tau(\hat{n})$ introduces secondary anisotropies in the CMB temperature on small scales. We analyzed current data from the WMAP and ACT observations, but found that the effect of patchy τ is too small to be seen in the TT power spectrum. We then showed that there exists a simple estimator constructed from the temperature maps, which is sensitive to small values of patchiness. The key idea is that the damping caused by inhomogeneous Thomson scattering *multiplies* the CMB temperature. Multiplication in angular space is equivalent to convolution in harmonic space which transfers power from low multipoles to high multipoles. Since most of the patchy τ contribution is on very small scales, we filtered the CMB map into low frequency and high frequency maps using HEALPix routines. We then computed the cross correlation between the squared maps, which we call the patchy τ correlator. We showed that the patchy τ component is clearly correlated with the primary CMB, while observations of the primary CMB on different scales are independent of each other. This technique is sensitive to patchiness values as small as $\tau_{\rm rms} \sim 0.003$ seen in our maps.

We then considered the more difficult question of identifying patchy reionization in the presence of other secondary components. One might hope to remove frequency dependent secondaries through a multi-frequency analysis of CMB maps. The Planck satellite measures the CMB in 9 frequency channels for $2 < l \lesssim 2000$, while the ACT experiment uses 2 frequency channels for $515 < l < 9750$ (Dunkley et al. 2011), and the SPT experiment uses 3 frequency channels for $675 < l < 9400$ (Keisler et al. 2011; Reichardt et al. 2012). The frequency independent contributions such as CMB lensing and kSZ are harder to remove. CMB lensing shows a non-zero correlation, but it is smaller than the correlation due to patchy τ and has a different dependence on the scale $l_{\rm boundary1}$. The kSZ shows no correlation with the primary CMB. We showed that patchy τ is easily detectable even when lensing and kSZ are included. It may also be possible to distinguish different reionization models based on the magnitude of the patchy τ correlator, even when they have the same value of $\langle \tau \rangle$, provided the $\tau_{\rm rms}$ values are different. On the other hand,

the large angle EE polarization may distinguish models with different $\langle\tau\rangle$, but is insensitive to $\tau_{\rm rms}$. The patchy τ correlator is thus a useful probe of reionization that provides information complementary to what may be obtained from the polarization power spectrum. With future data sets, one may hope to distinguish between different reionization histories by computing the cross correlation parameter in conjunction with the EE and the kSZ power spectra (a detailed treatment of the polarization and patchy kSZ power spectra is left to a companion paper (Battaglia et al. 2012a)).

We then included gaussian random noise in addition to lensing and kSZ in order to account for frequency dependent secondaries that are still present after a multi-frequency analysis has been employed to minimize the contribution from these components. We showed that a detection of patchy τ would require cleaning the small scale maps to a noise level $\lesssim 10$ μK/pixel. Such a low noise level would require a good understanding of the instrument as well as observations of the CMB at multiple frequencies in order to minimize frequency dependent contaminations. Finally we included the tSZ and the infrared and point source background to the maps, and attempted to identify the patchy τ signal. We showed that a plausible detection of patchy reionization may be made at low frequencies ~ 90 GHz.

Current and upcoming experiments are sensitive to low frequency channels and should be able to constrain extended reionization histories. Quantifying the patchiness of reionization could provide information regarding ionizing sources. Visbal & Loeb (2012) found that when ionization by X-rays is included, the patchy contribution is reduced owing to the larger mean free path of the ionizing photons. For a fixed mean optical depth $\langle\tau\rangle$, this implies a smaller reionization contribution from lower energy sources, and hence smaller values of $\tau_{\rm rms}$, influencing the patchy kSZ (Visbal & Loeb 2012), as well as the patchy τ correlator. Early reionization from other sources such as dark matter annihilation (Natarajan & Schwarz 2008, 2009, 2010) may also be probed in a similar way (Visbal & Loeb 2012). A more complete analysis is left to future work.

A.N. and N.B. are supported by a McWilliams postdoctoral fellowship awarded by the Bruce and Astrid McWilliams Center for Cosmology. We thank Christian Reichardt, Jonathan Sievers, Kendrick Smith, and David Spergel for helpful discussions. H.T. is supported in part by NSF grant AST-1109730. A.L. is supported in part by NSF grant AST-0907890, and NASA grants NNX08AL43G and NNA09DB30A. The simulations were performed at the Pittsburgh Supercomputing Center (PSC) and the Princeton Institute for Computational Science and Engineering (PICSciE). We thank Roberto Gomez and Rick Costa at the PSC and Bill Wichser at PICSciE for invaluable help with computing. Some of the results in this paper have been derived using the HEALPix (K.M. Górski et al., 2005, ApJ, **622**, p759) and LensPix (A. Lewis, 2005, Phys. Rev. D **71**, 083008) packages. We acknowledge the use of the Legacy Archive for Microwave Background Data Analysis (LAMBDA). Support for LAMBDA is provided by the NASA Office of Space Science.

REFERENCES

Barkana, R., & Loeb, A. 2001, Phys. Rep., 349, 125
—. 2004, ApJ, 609, 474
Battaglia, N., Natarajan, A., Trac, H., Cen, R., & Loeb, A. 2012a, (Paper III) in preparation
Battaglia, N., Trac, H., Cen, R., & Loeb, A. 2012b, (Paper I) in preparation
Becker, R. H. et al. 2001, AJ, 122, 2850
Blas, D., Lesgourgues, J., & Tram, T. 2011, J. Cosmology Astropart. Phys., 7, 34
Bleem, L. et al. 2012, Journal of Low Temperature Physics, 167, 859
Ciardi, B., Ferrara, A., & White, S. D. M. 2003, MNRAS, 344, L7
Das, S., & Bode, P. 2008, ApJ, 682, 1
Das, S. et al. 2011, ApJ, 729, 62
Doré, O., Holder, G., Alvarez, M., Iliev, I. T., Mellema, G., Pen, U.-L., & Shapiro, P. R. 2007, Phys. Rev. D, 76, 043002
Dunkley, J. et al. 2011, ApJ, 739, 52
—. 2009, ApJS, 180, 306
Dvorkin, C., Hu, W., & Smith, K. M. 2009, Phys. Rev. D, 79, 107302
Dvorkin, C., & Smith, K. M. 2009, Phys. Rev. D, 79, 043003
Fan, X. et al. 2001, AJ, 122, 2833
Fan, X., Narayanan, V. K., Strauss, M. A., White, R. L., Becker, R. H., Pentericci, L., & Rix, H.-W. 2002, AJ, 123, 1247
Górski, K. M., Hivon, E., Banday, A. J., Wandelt, B. D., Hansen, F. K., Reinecke, M., & Bartelmann, M. 2005, ApJ, 622, 759
Gunn, J. E., & Peterson, B. A. 1965, ApJ, 142, 1633
Hlozek, R. et al. 2012, ApJ, 749, 90
Hu, W. 2000, ApJ, 529, 12
Keisler, R. et al. 2011, ApJ, 743, 28
Kogut, A. et al. 2011, J. Cosmology Astropart. Phys., 7, 25
Lamarre, J.-M. et al. 2010, A&A, 520, A9
Larson, D. et al. 2011a, ApJS, 192, 16
—. 2011b, ApJS, 192, 16
Lesgourgues, J. 2011, ArXiv e-prints
Lewis, A. 2005, Phys. Rev. D, 71, 083008
Liu, G.-C., Sugiyama, N., Benson, A. J., Lacey, C. G., & Nusser, A. 2001, ApJ, 561, 504
Loeb, A., & Barkana, R. 2001, ARA&A, 39, 19
Mandolesi, N. et al. 2010, A&A, 520, A3
McQuinn, M., Furlanetto, S. R., Hernquist, L., Zahn, O., & Zaldarriaga, M. 2006, New A Rev., 50, 84
Mortonson, M. J., & Hu, W. 2010, Phys. Rev. D, 81, 067302
Natarajan, A., & Schwarz, D. J. 2008, Phys. Rev. D, 78, 103524
—. 2009, Phys. Rev. D, 80, 043529
—. 2010, Phys. Rev. D, 81, 123510
Niemack, M. D. et al. 2010, in Society of Photo-Optical Instrumentation Engineers (SPIE) Conference Series, Vol. 7741, Society of Photo-Optical Instrumentation Engineers (SPIE) Conference Series
Pentericci, L. et al. 2002, AJ, 123, 2151
Reichardt, C. L. et al. 2012, ApJ, 755, 70
Sehgal, N., Bode, P., Das, S., Hernandez-Monteagudo, C., Huffenberger, K., Lin, Y.-T., Ostriker, J. P., & Trac, H. 2010, ApJ, 709, 920
Sokasian, A., Abel, T., Hernquist, L., & Springel, V. 2003, MNRAS, 344, 607
Trac, H., Bode, P., & Ostriker, J. P. 2011, ApJ, 727, 94
Trac, H., Cen, R., & Loeb, A. 2008, ApJ, 689, L81
Tumlinson, J., & Shull, J. M. 2000, ApJ, 528, L65
Visbal, E., & Loeb, A. 2012, J. Cosmology Astropart. Phys., 5, 7
Weller, J. 1999, ApJ, 527, L1
Wyithe, J. S. B., & Loeb, A. 2003, ApJ, 588, L69
Zahn, O. et al. 2012, ApJ, 756, 65
Zahn, O., Zaldarriaga, M., Hernquist, L., & McQuinn, M. 2005, ApJ, 630, 657